ADVANCED OPTICAL MATERIALS
www.advopticalmat.de

Simple Encoded Circularly Polarized Protein Lighting

Stephanie Grümbel, Marco Hasler, Sara Ferrara, Marta Patrian, Jesús Agustín Banda-Vázquez, Pedro B. Coto, Juan Pablo Fuenzalida Werner, and Rubén D. Costa**

Lighting systems with circularly polarized luminescence (CPL) are an emerging field with high hopes in, for example, neural cell circuits and encoding applications. The major challenges that forfeits their real-world application are i) the design of chiroptical materials (CMs) with high CPL brightness (B_{CPL}; today's record is Eu-based compounds with average 287 $M^{-1}cm^{-1}$, while 90% of other CMs show <150 $M^{-1}cm^{-1}$ in solution) and ii) how to keep CPL response in films/coatings of technological relevance. Since natural evolution is driven by chiral selectivity at the supramolecular level, fluorescent proteins (FPs) are ideal candidates to provide large B_{CPL} spanning visible and near-infrared regions. This hypothesis is confirmed for all the known FP classes, demonstrating high emission intensities (photoluminescence quantum yields (ϕ) up to 76%) and record average B_{CPL} of |200| $M^{-1}cm^{-1}$ (solution). What is more, the CPL response is also kept in polymer coatings. It is rationalized that structural factors (chromophore rigidity, surrounding amino acids, supramolecular packaging, and exciton coupling) hold a significant influence, regardless of the ϕ values. Finally, proof-of-concept CPL-encoded signals in monochromatic/white hybrid light-emitting diodes with FP-polymer filters show exceptional stabilities. Overall, this work stands out FPs toward a new CM family, in general, and biogenic CPL-encoded lighting systems, in particular.

1. Introduction

Chiroptical materials (CMs) based on chiral luminophores that emit circularly polarized luminescence (CPL) are essential for next-generation photonics, as they can be applied to i) enantioselective polymerization, ii) guided development of neural cells and circuits, iii) thin-film lighting, and iv) smart sensing materials for object identification, among others.[1–5] However, this emerging field is limited by three major aspects: i) the existence of a limited number of materials that combine efficient CPL with high photoluminescence quantum yields (ϕ) and molar extinction coefficients (ε), ii) low photo-stabilities and difficult handling of polymer coatings keeping CPL response for technology, and iii) lack of eco-designed CM synthesis routes and/or materials.[6,7] In detail, most native CMs show CPL brightness values <10 $M^{-1}cm^{-1}$ (i.e., B_{CPL} as a product of ε, ϕ, and the dissymmetry factor (g_{lum}) as shown in Equation (1)[8–10]

$$B_{CPL} = \Phi \times \varepsilon \times \frac{g_{lum}}{2} \quad (1)$$

where B_{CPL} is the circularly polarized luminescence brightness, ϕ is the photoluminescence quantum yield, ε is the molar extinction coefficient and g_{lum} is the dissymmetry factor.

Recently, efforts on designing CMs has followed two main paths: i) small organic compounds (i.e., ketones, cyclophanes, BODIPYs, helicenes and helicenoids, pyrene intramolecular excimers) at the common cost of extensive synthesis routes with low yields and hard purification processes to avoid enantiomeric excess in concert with low ϕ and g_{lum},[10,11] and ii) complexes (i.e., d-metal and rare earth compounds) sacrificing ε, processability, and sustainability for high g_{lum}.[6,10] In summary, >90% of published CM families show average B_{CPL} values <150 $M^{-1}cm^{-1}$ (e.g., ketones: 1.1 × 10^{-3} $M^{-1}cm^{-1}$, cyclophanes: 67 $M^{-1}cm^{-1}$; BODIPYs: 47 $M^{-1}cm^{-1}$; helicenes: 18.7 $M^{-1}cm^{-1}$; pyrene excimers: 127 $M^{-1}cm^{-1}$; d-metal compounds: 29.7 $M^{-1}cm^{-1}$; Tb-based compounds: 146.4 $M^{-1}cm^{-1}$; Yb-based compounds: 3.75 $M^{-1}cm^{-1}$) with only Eu-based compounds holding today's record average B_{CPL} of 287 $M^{-1}cm^{-1}$.[10] In this context, supramolecular assemblies and liquid crystals have been

S. Grümbel, M. Hasler, S. Ferrara, M. Patrian, J. A. Banda-Vázquez, J. P. Fuenzalida Werner, R. D. Costa
Chair of Biogenic Functional Materials
Technical University of Munich
Schulgasse, 22, 94315 Straubing, Germany
E-mail: jpf.werner@tum.de; ruben.costa@tum.de

P. B. Coto
Materials Physics Center (CFM)
Spanish National Research Council (CSIC)
Donostia International Physics Center (DIPC)
Paseo Manuel de Lardizabal 5, Donostia-San Sebastián (Gipuzkoa) 20018, Spain

The ORCID identification number(s) for the author(s) of this article can be found under https://doi.org/10.1002/adom.202400106

DOI: 10.1002/adom.202400106

widely studied, achieving impressive g_{lum} values, an almost full polarization, and B_{CPL} values as high as 300 $M^{-1}cm^{-1}$ for supramolecular assemblies, as leading example.[12–15]

Finally, most of these B_{CPL} values refer to studies in diluted solutions, as it is not easy to calculate the effective absorption efficiency in aggregated, supramolecular, and solid-state samples. More specifically, CPL response measurements in thin-films and/or self-standing coatings of relevance for technological applications are challenged by aggregation-emission quenching causing low ϕ and high scattering rendering low g_{lum}. At the same time, the impact of irradiation stress on the CPL signal has not been addressed.[16–18] Thus, ideal highly efficient CMs and their respective materials fulfilling the Green Photonics targets have not been met yet.[19]

In view of this scenario, we start investigating fluorescent proteins (FPs) as a potential biogenic CM family encouraged by three aspects: i) natural evolution is driven by chiral selectivity at the supramolecular level and, in turn, FPs could be considered as ideal natural emitters to provide large B_{CPL} spanning visible and near-infrared regions, ii) their cost-effective bacterial production and easy recyclability and/or degradability, and iii) the recent advances on stabilizing FPs in polymer-coatings for high-end use in optoelectronics and photonics.[20–23] Thus, FPs have successfully crossed the bridge from biology to material science as an emerging approach for i) polymer and solution color converting filters applied to hybrid light-emitting diodes (HLEDs),[24,25] solar concentrators,[26] data storage,[27] test samples for imaging validation,[23] etc., ii) color sources in exciton-polariton lasers,[28] and iii) easy to engineer materials in photochromic molecular sensing.[23,29]

Herein, we demonstrate that FPs are a new relevant family of biogenic CMs by evaluating the CPL response of all the known classes of FPs covering the visible and near-infrared regimes (i.e., ligand-based and β-barrel FPs; **Figure 1**), reaching record average B_{CPL} values of $|200|$ $M^{-1}cm^{-1}$ (vide supra). What is more, theoretical and structural analyses enabled us to elucidate the complex interplay of parameters (i.e., ϕ, chromophore rigidity, surrounding amino acids, aggregation, and exciton coupling) ruling the CPL response. In this respect, positive and negative CPL signals have been noted in FPs with covalently bound biliverdin (BV) chromophores, depending on their structural conformation. In β-barrel FPs, B_{CPL} reaches a remarkable value of −425 $M^{-1}cm^{-1}$ for the green-emitting protein mGreenLantern (mGL) and −239 $M^{-1}cm^{-1}$ for the red-emitting *Discosoma* red fluorescent protein (DsRed). This CPL response is attributed to the excited state chirality of the isolated chromophore (threonine – tyrosine – glycine; TYG),[30] which features orders of magnitude reduced ϕ compared to that of the respective FP, but a similar g_{lum}. Finally, we capitalize on our know-how in stabilizing FPs in self-standing polymer coatings for photon manipulation in HLEDs to encode monochromatic and white CPL signals in blue, green, amber, and white HLEDs without affecting their color and luminous efficiency.

In view of all the aforementioned, this work sets in FPs as a new family of biogenic CMs with a remarkable average B_{CPL}, easy processability in thin-films that are, in addition, easy-to-apply to encode CPL signal in monochromatic and white protein-based hybrid lighting systems.

2. Results and Discussion

2.1. CPL Response of Ligand-Based FPs in Solution

Since induced CPL via supramolecular chiral templating is a known phenomenon,[13] we first focus on natural ligand-based FPs in which the protein scaffold offers a binding pocket for natural chromophores. Here, the best representative examples are FPs binding bilin-like chromophores (i.e., bilirubin (BR) and biliverdin (BV); Figure 1a–c).[31,35–37] According to the literature, BR shows a weak CPL emission when it is artificially docked into a human serum albumin (HSA) protein featuring a g_{lum} of 1×10^{-3} and B_{CPL} <1 $M^{-1}cm^{-1}$.[8,9,38] In contrast, BR alone or in the presence of bovine serum albumin (BSA) did not show a CPL response.[8] From all FPs reported to date, UnaG is the only one that bears BR as chromophore[31,37] and features a clear differential CPL emission between left and right circularly polarized emission (**Figure 2**a,b), reaching superior values of g_{lum} of -1.3×10^{-2} and B_{CPL} of −246 $M^{-1}cm^{-1}$ compared to the BR-HSA complex (**Table 1**). Interestingly, the negative CPL signal indicates a right-handed helical conformation of the excited sate of BR[9,38,39] that contrasts with a positive CPL signal of the BR-HSA complex.[9] This was nicely confirmed upon analyzing the crystal structure of both proteins. As shown in Figure 2c,d, the locked conformation of BR reported for UnaG is exactly the opposite conformer found for BR-HSA.[31,37] Circular dichroism (CD) measurements also confirmed that the conformation in the crystal structure matches the conformation in solution (Figure S1a, Supporting Information). Specifically, UnaG shows a more prominent g_{lum} in the ground state and the opposite CD signal with respect to the BR-HSA complex.[9,40] According to the classical understanding, the CPL signal of small organic molecules is opposed to ϕ as it is based on electronically forbidden transitions.[41] Therefore, it is surprising that UnaG with ϕ ∼50% features a more prominent CPL than that of the BR-HSA complex with a ϕ <1%.[40] But, compared to small organic molecules in solution, the chromophores of FPs are buried and partially locked through bonded and non-bonded interactions with the surrounding amino acids in a spatially organized protein cavity. This strongly determines the optical properties of the chromophore with protein scaffolds being able to induce ground state chirality,[42] and other biopolymers, like DNA, triggering CPL features in non-chiral molecules.[43] This suggests that the chiral environment offered by the protein backbone is able to keep BR in a highly emissive conformation and to induce structural distortions that increase its chiral character. Interestingly, it is worthwhile to mention that Nagata et al. demonstrated that the inverse relation between ϕ and CPL is not clearly present in most of the experimental data available.[11]

Next, FPs containing BV, such as smURFP and iRFP720, were also studied. BV ground state chirality in solution and bound to proteins, like HSA, has been widely studied, but the CPL response has not been disclosed.[8,9,38] In this respect, we noted a positive CPL signal for smURFP with a g_{lum} of 5.0×10^{-3} and B_{CPL} of 76 $M^{-1}cm^{-1}$, while iRFP720 shows a negative CPL signal with a g_{lum} of -1.3×10^{-2} and B_{CPL} of −20 $M^{-1}cm^{-1}$ (Table 1 and Figure 2e,f,h,i). This is also in line with the positive and negative CD absorption features at low energies (Q-bands) of

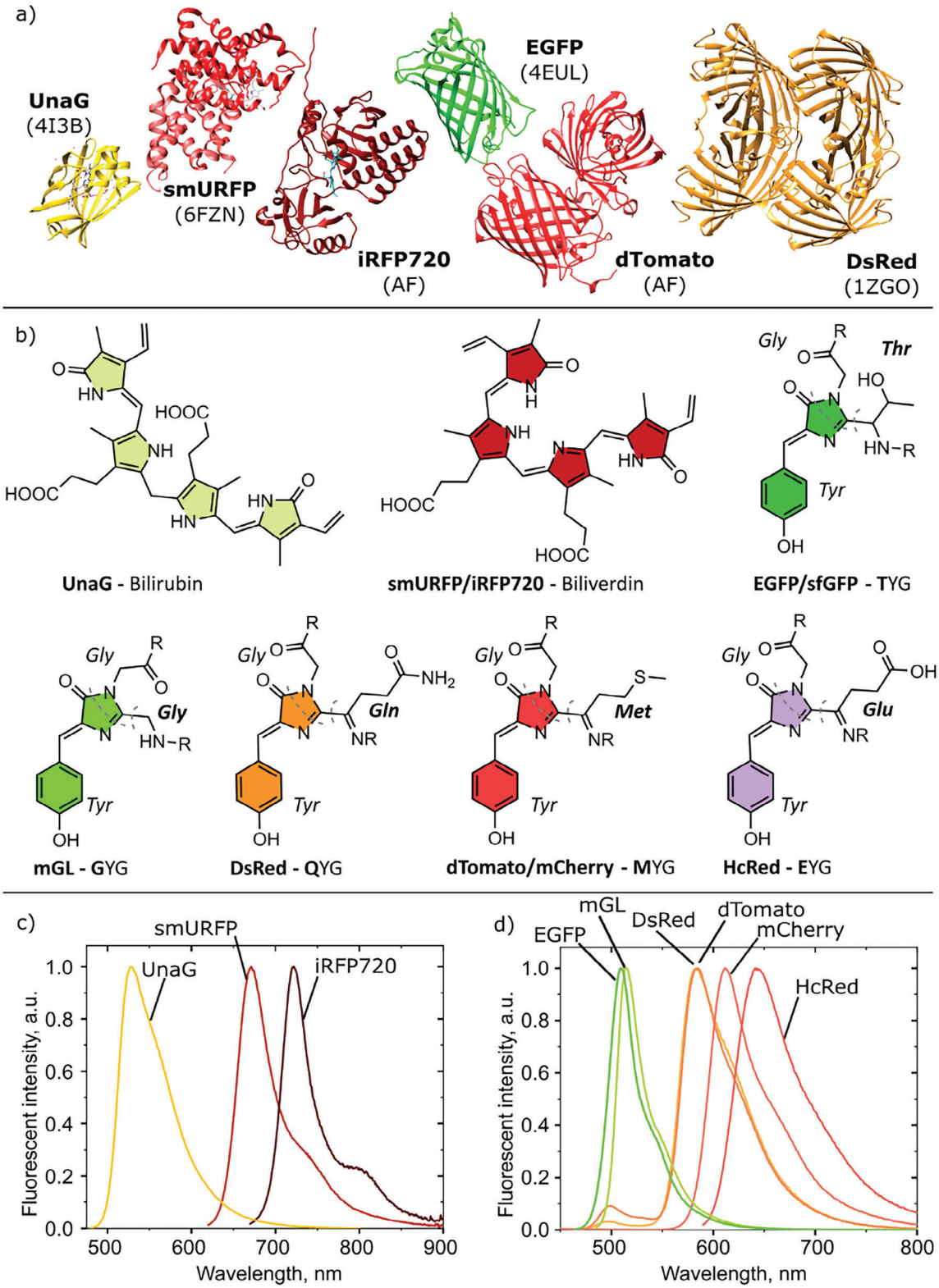

Figure 1. a) Exemplary structures of FPs covering visible and near-infrared regions: UnaG (Protein Data Bank (PDB: 4I3B[31])), smURFP (PDB: 6FZN[32]), iRFP720 (AlphaFold (AF) prediction), EGFP (PDB: 4EUL[33]), dTomato (AF) and DsRed (PDB: 1ZGO[34]). b) Chromophores of ligand-based FPs: Bilirubin in UnaG, biliverdin in smURFP, and iRFP720 as well as the chromophore in β-barrel FPs autocatalytically formed by the following amino acids threonine (T, Thr), tyrosine (Y, Tyr), glycine (G, Gly), methionine (M, Met), glutamic acid (E, Glu) and glutamine (Q, Gln). c,d) Exemplary of the emission spectra of ligand-based FPs (c) and β-barrel FPs (d) in aqueous phosphate buffered saline (PBS) solution.

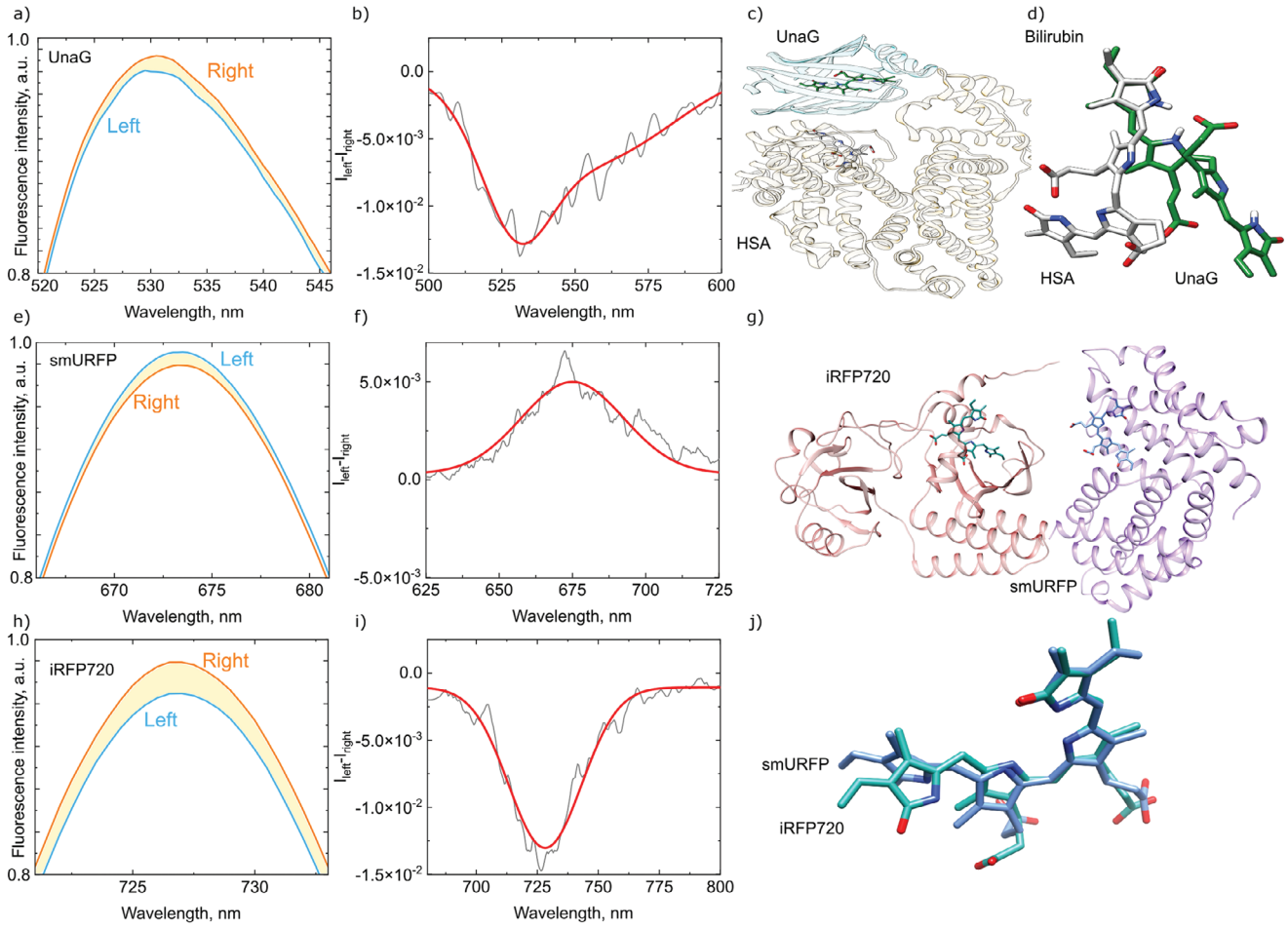

Figure 2. UnaG: a) left and right circularly polarized emission spectra, b) CPL signal in aqueous PBS buffer solution, c) crystal structures of UnaG (blue, PDB: 4I3B[31]) and HSA (gold, PDB: 2VUE[44]) binding BR, and d) comparison between the locked conformation of BR bound by UnaG (green, PDB: 4I3B[31]) and HSA (silver, PDB: 2VUE[44]) obtained from their respective crystal structures. smURFP: e) left and right circularly polarized emission spectra, f) CPL signal in aqueous PBS buffer solution, and g) crystal structure of smURFP (PDB: 6FZN,[32] purple) and AF model of iRFP720 (salmon). iRPFP720: h) left and right circularly polarized emission spectra, i) CPL signal in aqueous PBS buffer solution, and j) comparison between the locked conformation of BV bound to smURFP (blue, PDB: 6FZN[32]) and iRFP720 (turquoise, PDB:8AFK[45]) obtained from their respective crystal structures.

smURFP and iRFP720, respectively (Figure S1b,c, Supporting Information). This has been attributed to different chromophore conformations induced by the protein cavity (Figure 2g,j).[32] The fact that iRFP720 shows a g_{lum} value three times higher than that of BV in smURFP could be attributed to i) the interplay between the chromophore and the protein scaffold that imposes rigidity constraints, induces cavity polarity effects, and determines the degree of exposition of the chromophore to the surrounding solvent, and ii) exciton coupling between chromophores since both proteins are dimers.[13] The latter is ruled out, since their CD absorption spectra neither exhibit Davydov splitting at the Soret bands (biphasic negative and positive CD bands) nor any peak shift (Figure S1b,c, Supporting Information).[46–48] Indeed, the smURFP dimer only contains one BV, while the distance

Table 1. Photo- and circularly polarized luminescence parameters of the ligand-based FPs containing BV and BR chromophores in PBS buffer solutions.

FP	Chr[a)]	ε [M^{-1} cm^{-1} × 10^3][b)]	λ_{ex} [nm][c)]	λ_{em} [nm][d)]	ϕ [%][e)]	$\tau_{375\ nm}$ [ns][f)]	g_{lum} 10^{-2}[h)]	B_{CPL} [M^{-1} cm^{-1}][i)]	A_{Left}-A_{right} 10^{-2}[j)]
UnaG	BR	77.3	497	528	49.0	2.34[g)]	−1.3	−246	−0.3
smURFP	BV	180	644	671	16.9	1.73[g)]	0.5	76	1.9
iRFP720	BV	96.0	702	722	3.16	0.74	−1.3	−20	−1.4

[a)] Chromophore of the proteins, bilirubin (BR) or biliverdin (BV); [b)] Molar extinction coefficient; [c)] Excitation wavelength maximum; [d)] Emission wavelength maximum; [e)] Photoluminescence quantum yield; [f)] Excited state lifetime at 375 nm; [g)] Average excited state lifetime; [h)] Dissymmetry factor; [i)] CPL brightness; [j)] CD emission difference of left – right.

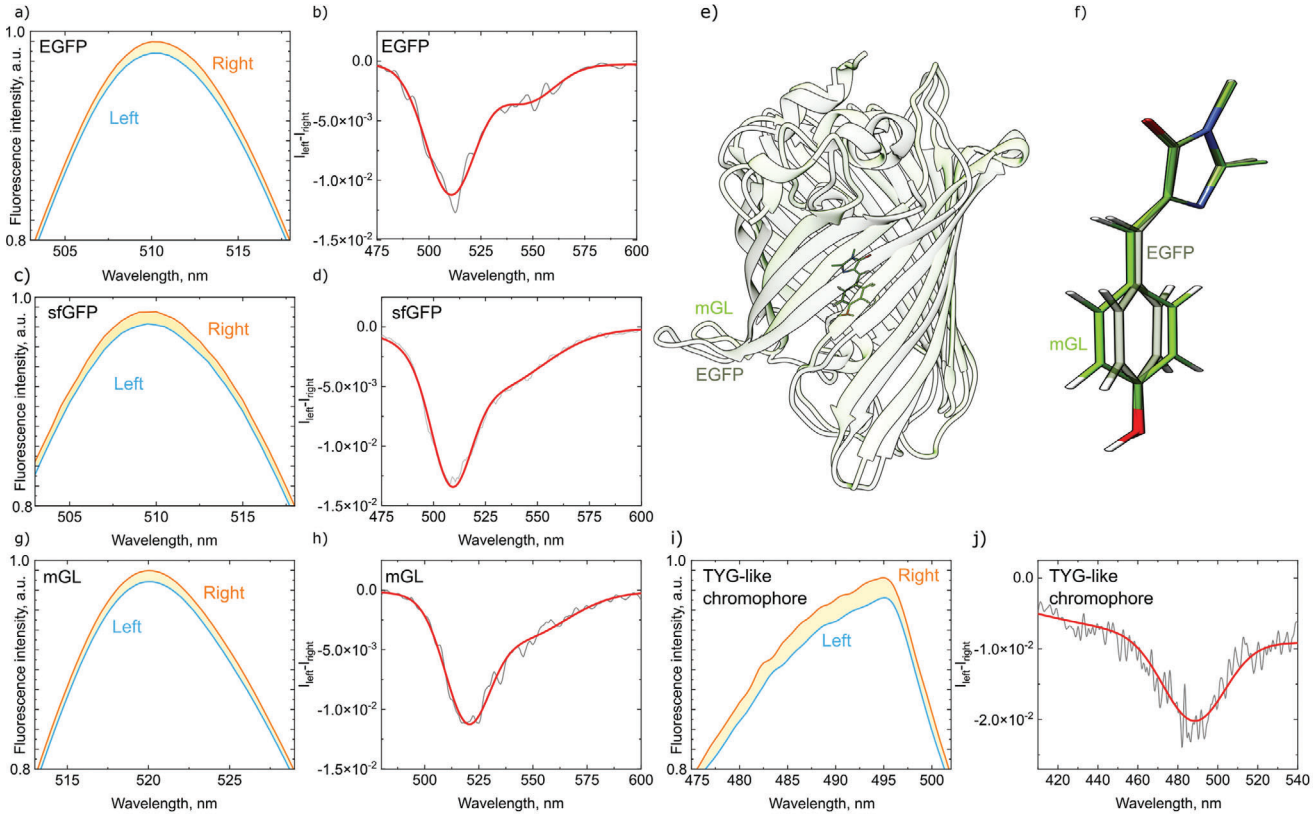

Figure 3. EGFP: a) left and right circularly polarized emission spectra and b) CPL signal in aqueous PBS buffer solution. sfGFP: c) left and right circularly polarized emission spectra and d) CPL signal in aqueous PBS buffer solution. mGL: e) protein structure (AF), f) overlap of the chromophore structure of EGFP (gray, PDB: 4EUL[33]) and mGL (green, AF), g) left and right circularly polarized emission spectra and h) CPL signal in aqueous PBS buffer solution. TYG-like chromophore: i) left and right circularly polarized emission spectra and j) CPL signal in glycerol and NaOH.

between BV chromophores exceeds the classical range for exciton coupling in iRFP720.[49] Thus, the different BV environments are key. Here, a significant difference is that iRFP720 provides a more tightly packed surrounding than smURFP, as for typical bacterial phytochromes like iRFP720, the buried surface area is ca. 90%, while smURFP features a buried surface of ca. 70%.[32,50] Indeed, the more exposed and motile BV chromophore has also been used to justify the blue-shifted emission in smURFP.[32] Thus, the higher g_{lum} response in iRFP720 might be related to a more tightly packed surrounding that induces a more prominent chiral character to the BV.[42,43]

2.2. CPL Response of β-Barrel FPs in Solution

We next focus on determining the CPL response of the enhanced green fluorescent protein (EGFP) and its structural analogs, FPs whose chromophore is autocatalytically formed inside the protein β-barrel. In short, EGFP exhibits a g_{lum} of -1.1×10^{-2} and B_{CPL} of -208 $M^{-1}cm^{-1}$ (**Figure 3a,b** and **Table 2**) that is in line with our data concerning ground state chirality (Figure S2a, Supporting Information) and the previously reported CD data.[46] As a comparison, we also characterized superfolder GFP (sfGFP) and mGreenLantern (mGL), as they all share similar emission features with respect to maximum emission wavelength and emission band shape (Figure 1d and Table 2). sfGFP exhibits a reduced ϕ (56%) and enhanced g_{lum} (-1.3×10^{-2}) and ε (83300 $M^{-1}cm^{-1}$) values that resulted in an overall better B_{CPL} of -304 $M^{-1}cm^{-1}$ (Figure 3c,d and Table 2).[51] mGL shows a different chromophore (GYG) but a similar 3D structure to EGFP (Figure 3e,f; Figure S3, Supporting Information).[52] This chromophore gifts mGL with almost a double ε and a superior ϕ (76%) compared to those of EGFP,[33,52] but similar g_{lum} (-1.1×10^{-2}). This resulted in a much higher B_{CPL} of -425 $M^{-1}cm^{-1}$ (Figure 3g,h and Table 2), the highest reported value for an organic emitter.[10]

Interestingly, there is no clear relationship between ϕ and g_{lum} values in these three green-emitting FPs. The origin of the CPL signal in the three proteins can be assigned to that of their chromophore. Ground state chirality of the isolated chromophore of EGFP has been theoretically shown[53] and we have also studied the excited state chirality of the isolated TYG-like chromophore, noting a ϕ <1% and a g_{lum} of -1.8×10^{-2} (Figure 3i,j and Table 2; Figure S4, Supporting Information). The g_{lum} values are in the same range as those noted for EGFP, sfGFP, and mGL, but the ϕ values of these proteins are significantly higher than that of the TYG-like chromophore. To get insight into the chiroptical properties of the TYG-like chromophore in the excited state, we have carried out relaxed scans along the dihedral angles α and β (Figure S4, Supporting Information) using time-dependent

Table 2. Photo- and circularly polarized luminescence parameters of TYG-like chromophore and β-barrel FPs in aqueous PBS buffer solutions as well as the average dielectric on chromophore pocket and the interplane angles.

FP	Chr[b)]	ε [M^{-1} cm^{-1} × 10^3][c)]	λ_{ex} [nm][d)]	λ_{em} [nm][e)]	ϕ [%][f)]	τ_{375nm} [ns][g)]	g_{lum} 10^{-2}[i)]	B_{CPL} [M^{-1} cm^{-1}][j)]	A_{Left}-A_{right} x 10^{-2}[k)]	ADCP[l)]	IPA[m)]
TYG-like chromophore[a)]	–	–	444	500	<1	0.59[h)]	−1.8	–	–	–	–
EGFP	TYG	55.9	488	510	67.8	3.31[h)]	−1.1	−208	−0.07	15.3	8.50
sfGFP	TYG	83.3	487	510	56.2	3.15	−1.3	−304	−0.22	15.3	7.44
mGL	GYG	101.8	500	515	75.9	3.36	−1.1	−425	−0.38	16.0	6.26
DsRed	QYG	72.5	559	584	73.2	3.80	−0.9	−239	−0.29	16.6	5.47
HcRed	EYG	20.0	606	651	5.49	1.07	−1.5	−8.24	−0.47	16.3	7.64
mCherry	MYG	72.0	585	612	22.9	1.63	−1.5	−124	−0.50	17.0	18.1
dTomato	MYG	69.0	555	583	70.2	3.60	−1.3	−315	−0.34	17.0	18.1

[a)] In glycerol and NaOH; [b)] Amino acid composition of the chromophore; Threonine (T), tyrosine (Y), glycine (G), glutamine (Q), glutamic acid (E), and methionine (M); [c)] Molar extinction coefficient; [d)] Excitation wavelength maximum; [e)] Emission wavelength maximum; [f)] Photoluminescence quantum yield; [g)] Excited state lifetime excited at 375 nm; [h)] Average excited state lifetime; [i)] Dissymmetry factors; [j)] CPL brightness; [k)] Difference of the CD emission of left – right; [l)] Average dielectric on chromophore pocket (5 Å); [m)] Interplane angles range.

density functional theory (TD-DFT).[54] This allowed us to simulate the impact that the excited state relaxation of the chromophore in a frozen environment has on its chiroptical properties (Discussion S1 and Tables S1–S6, Supporting Information). The results show that small geometrical distortions trigger the emergence of a sizeable rotational strength. This suggests that the chiral environment offered by the protein scaffold could keep a significant CPL response, while locking the chromophore structure in a *cis* conformation to exert a high ϕ. This exemplifies that ϕ and g_{lum} are not clearly linked in FPs, but could be tuned by structural factors of the protein cavity. For example, mGL features a higher ϕ than EGFP, but the same g_{lum}, though the ground state chirality for EGFP is nearly an order of magnitude lower than for mGL (Figure S2a,c, Supporting Information). Here, the sign of the ground state chirality and CPL for the isolated TYG-like chromophore, mGL, sfGFP, and EGFP confirms that the radiative active structure of the chromophore should be in a *cis* conformation (Figure S2, Supporting Information). Rosetta energy minimization of 1000 structures showed that mGL with the higher B_{CPL} value has the most pronounced *cis* conformation possible, followed by sfGFP and EGFP with minimum interplane angles range of 6.3, versus 7.4 and 8.5 degrees. This is also in line with the lower B_{CPL} for sfGFP and EGFP compared to mGL (Table 2; Figure S5, Supporting Information). Thus, we hypothesize that mGL can hold its CPL values as the protein scaffold might promote a more effective *cis* conformation to keep high ϕ and g_{lum} values compared to sfGFP and EGFP. However, we must also consider the interplay of the transition dipole moments that defines CPL response, as indicated in Equation (2)

$$g_{lum} = \frac{I_L - I_R}{\frac{1}{2}\left(I_L + I_R\right)} = \frac{4\,|\mu|\,|m|\cos\theta}{|\mu|^2 + |m|^2} \quad (2)$$

Here g_{lum} is the dissymmetry factor, I_L and I_R are the fluorescence intensity of left- and right-circularly polarized light, respectively. μ is the electric transition dipole moment, m is the magnetic transition dipole moment and θ is the angle between both vectors.[10,41]

Indeed, our TD-DFT calculations on the isolated TYG-like chromophore (Discussion S1, Supporting Information) showed that an increase in environmental polarity impacts both transition dipole moments with a major effect on the electric transition dipole moment.[55] In this context, mGL also offers a more polar environment (Table 2) when compared to EGFP. Thus, both, the environmental polarity of the protein cavity and a more prominent *cis* conformation, might rule the magnitude of g_{lum} and ϕ, resulting in remarkable B_{CPL} values; though a more thoughtful investigation must be focused on disentangling the impact on the magnetic transition dipole moment.

As a final step, we studied the CPL response of low-energy emitting FPs that are represented by mCherry, dTomato, DsRed, and HcRed.[56–58] Thanks to the tetrameric character of DsRed and HcRed, their chromophores (QYG and EYG, respectively) exhibit an exciton coupling between protein subunits, leading to a significant red-shifted emission (Figure 1a,b,d and Table 2).[46,59–61] However, they feature different photoluminescence and CPL characteristics. In short, DsRed shows a ϕ of 73%, g_{lum} of -9.0×10^{-3}, and B_{CPL} of -239 M^{-1} cm^{-1} (**Figure 4**a,b), while HcRed provides a ϕ of 5.5%, g_{lum} of -1.5×10^{-2}, and B_{CPL} of -8.2 M^{-1} cm^{-1} (Figure 4c,d). The two tetrameric proteins show a high degree of sequence similarity (Figure S6, Supporting Information); however, DsRed has around one-half of the ground state chirality signal intensity of HcRed (Table 2; Figure S7a,b, Supporting Information). While some correlation between ground state chirality and CPL could be noted, this does not explain the good CPL signal despite the significantly high ϕ value of DsRed. Here, there is a clear exciton peak in the CD absorption spectrum of DsRed, that is, the presence of the Davydov splitting at the chromophore peak and the shift on the transition maxima. In contrast, CD absorption spectrum of HcRed does not show the Davydov splitting feature (Figure S7a,b, Supporting Information).[46–48] While DsRed high probability of radiative decay could decrease the chances of exhibiting significant CPL, the exciton coupling in a chiral environment could, therefore, support its presence.[13,43]

The DsRed chromophore is more prone to be in *cis* conformation with a minimum interplane angle range of 5.5 versus

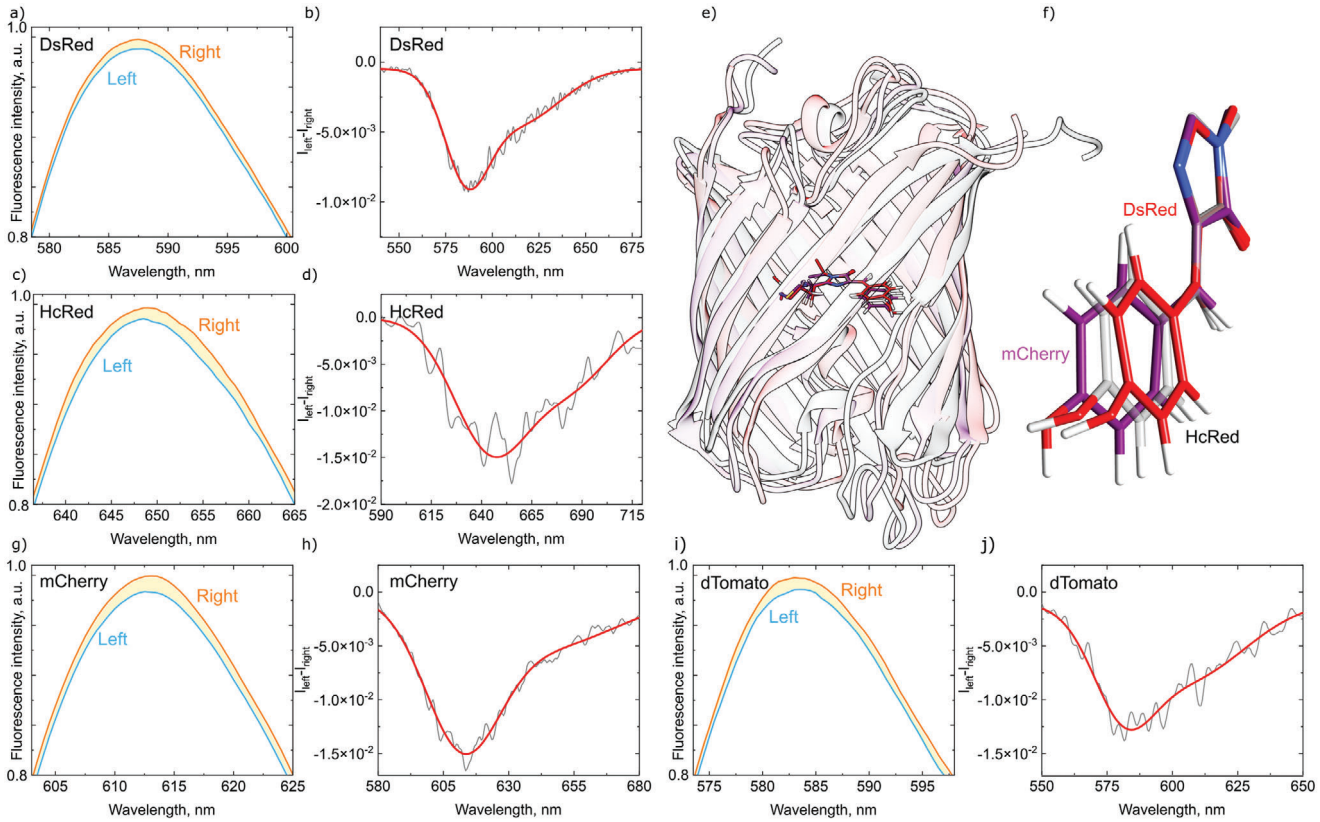

Figure 4. DsRed: a) left and right circularly polarized emission spectra and b) CPL signal in aqueous PBS buffer solution. HcRed: c) left and right circularly polarized emission spectra, d) CPL signal in aqueous PBS buffer solution, e) overlap of the structure of DsRed (red, PDB: 1ZGO[34]), HcRed (grey, PDB: 1YZW[62]) and mCherry (purple, PDB: 2H5Q[63]), f) overlap of the chromophore of DsRed (red), HcRed (grey) and mCherry (purple). mCherry: g) left and right circularly polarized emission spectra and h) CPL signal in aqueous PBS buffer solution. dTomato: i) left and right circularly polarized emission spectra and j) CPL signal in aqueous PBS buffer solution.

7.6 degrees for HcRed. Further, it is in a more polar environment than the chromophore of HcRed (Table 2 and Figure 4e,f). Thus, the interplay of these factors most likely assists DsRed in keeping its CPL response despite the high ϕ, allowing it to reach a very high B_{CPL}, one of the highest ever reported for a red emitter.[10]

We further investigated the monomeric and dimeric proteins derived from DsRed; mCherry and dTomato bearing a MYG chromophore.[56,57] mCherry featured a ϕ of 23% and g_{lum} of -1.5×10^{-2}, while dTomato has a higher ϕ of 70% and a similar g_{lum} of -1.3×10^{-2}. Ground state chirality of dTomato is around one-half of mCherry (Table 2; Figure S7c,d, Supporting Information) and, in turn, neither ground state chirality nor ϕ correlates with the high g_{lum} of dTomato compared to mCherry, or with their ancestor DsRed. As per our calculations, the structural model of dTomato shows a chromophore that has a similar likelihood to be in a *cis* conformation as the one for mCherry, but both show less likelihood *cis* conformation than DsRed (Table 2 and Figure 4e–j). However, the polarity of the cavity is significantly higher for dTomato and mCherry with respect to DsRed (Table 2). Here, a remaining parameter is the mCherry *β*-barrel flexibility, leading to a large volume of the binding pocket and a strong influence of the surrounding environment on the chromophore.[64,65]

As described above, the chromophores of red- and green-emitting structural analogs of GFP (GLPs), all *β*-barrel FPs, are generally found in the *cis* conformation, allowing the proteins to fluoresce. However, not all the GLPs stabilize the same *cis* conformation or to the same degree as our calculation shows (Table 2). Additionally, some proteins can fit a non-fluorescence *trans* conformation.[66] Thus, the volume of the binding pocket and the interactions with the chromophore define its chiral conformation. Our data show that CPL in GLPs arises from the chiral *cis* conformation present in the ground state, which is preserved in the excited state in all the evaluated GLPs. Further, variations in the electric transition dipole moment, determined by the inner polarity of the *β*-barrel and conformation of the chromophore, have been associated with chromophore packing as a critical parameter.[63,67] Our data shows that proteins with high ϕ and g_{lum}, consequently large B_{CPL}, like DsRed, dTomato, and mGL, provide a more polar environments to their chromophores than their counterparts with less ϕ and similar or lower g_{lum}.

To further clarify the effect of environment polarity on the CPL signal of FPs, we used mCherry as target system. Due to its *β*-barrel unique structure, which is less densely packed compared to green or tetrameric *β*-barrel FPs, it allows for

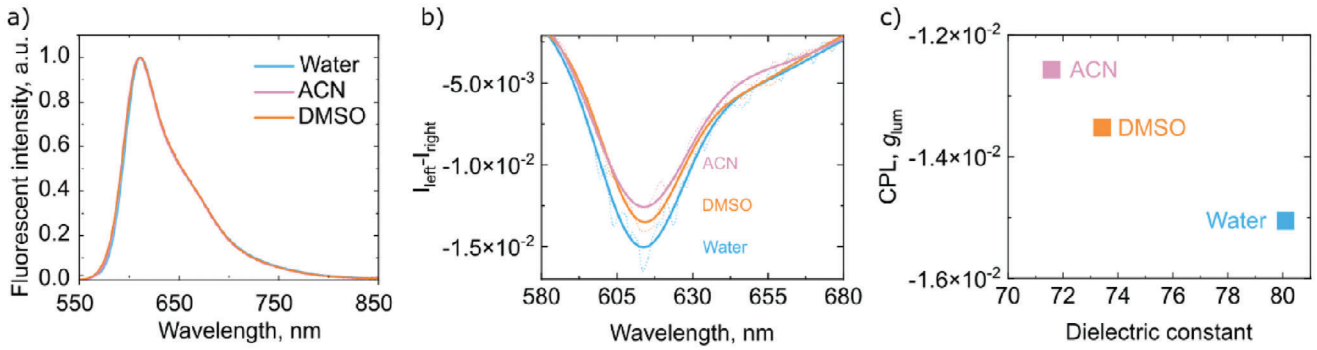

Figure 5. a) Emission spectra, b) CPL emission of mCherry in different solvent mixtures (water: blue, ACN: pink, DMSO: orange), and c) the correlation between the dielectric constant of the solvent and g_{lum}.

enhanced interaction between the chromophore and its surrounding environment.[64,65] This distinction facilitates the interaction of the solvent molecules with the protein chromophore. We evaluated the CPL intensity of mCherry across various solvent polarities by incorporating 20% acetonitrile (ACN) and dimethyl sulfoxide (DMSO), as detailed in **Figure 5** and Table S7 (Supporting Information). The concentrations were selected not to affect the tridimensional structure of the protein (Figure S8 and Table S7, Supporting Information). As shown in Figure 5a, the emission spectra of mCherry did not change with the different environment polarity, but a reduction in CPL intensity that further associates with a decrease in the radiative decay constant (Figure 5b,c). This is in line with Equation (2),[10,41] where CPL arises from the interplay between magnetic and electric transition dipole moments. Changes in environmental polarity will exert a significant impact on the electronic structure of the chromophore affecting the magnitude of both the electric and magnetic transition dipole moments, thereby altering the intensity of the CPL as expected.[68,69]

2.3. CPL Response of β-Barrel FPs in Materials

mGL and DsRed were further implemented in polarizer polymer coatings as they featured the highest B_{CPL} values (vide supra), high compatibility with polymers, and known photostability for lighting purposes.[52,70] As polymer matrix, we select hydroxypropyl cellulose (HPC) that has already been used for i) FP-lighting devices,[71] ii) CPL applications due to the chiral nematic structure,[72–74] and iii) CPL enhancing of small molecules and carbon dots.[16,75] Self-standing films of arbitrary shapes are easily prepared as reported elsewhere (see Experimental Section).[71] Here, we focus on large area films of 2 cm diameter containing 0.25, 0.5, and 1 mg of each FP (**Figure 6**).

At first, we evaluated the thermodynamic stability of mGL in HPC matrix (Figure S9b,c, Supporting Information). Modulated scanning fluorimetry shows that neither the melting temperature (T_m) nor the non-reversible folding temperature (T_{nr}) was drastically affected by the HPC matrix, confirming their compatibility. Further confirmation came from spectroscopic studies (Figure 6

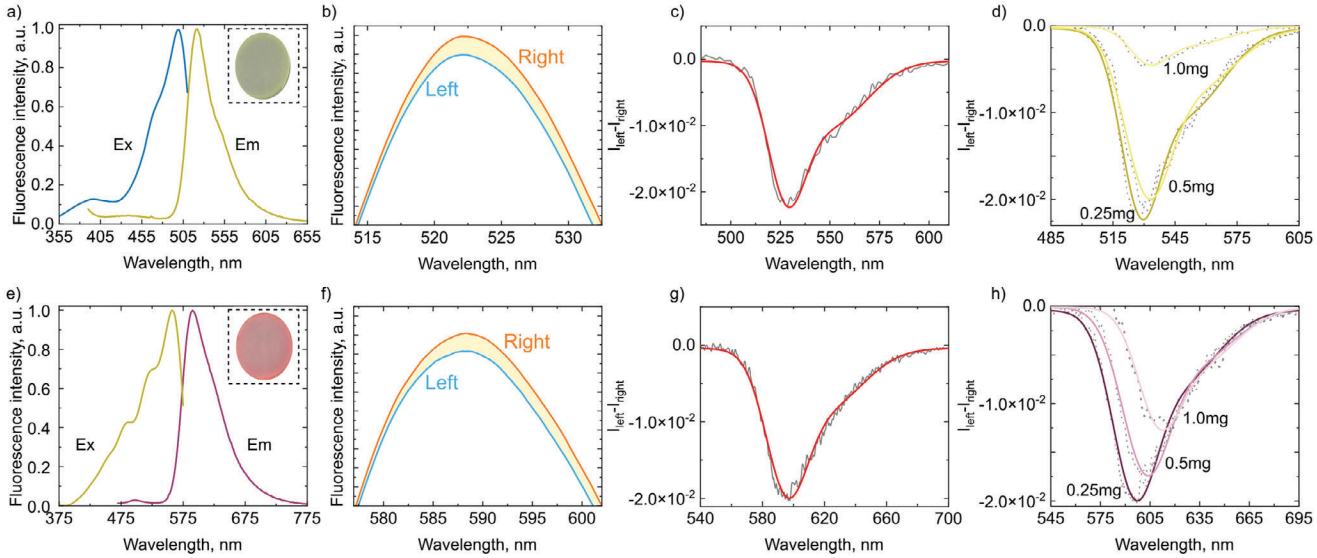

Figure 6. a,e) Excitation (Ex) and emission (Em) spectra as well as film photographs (insert). b,f) Left and right circularly polarized emission and c,g) CPL signal for mGL (top) and DsRed (bottom) in HPC films with 0.25 mg of each FP. d,h) Changes of CPL signal upon increasing the FP loading for mGL (top) and DsRed (bottom).

Table 3. Photo- and circularly polarized luminescence parameters of mGL and DsRed in aqueous PBS buffer solution (reference**) and in coatings with different FP loading.

FP-polymer	λ_{ex} [nm][a)]	λ_{em} [nm][b)]	ϕ [%][c)]	τ_{450nm} [ns][d)]	g_{lum} 10^{-2}[f)]
mGL **	500	515	76	3.20[e)]	−1.1
mGL 0.25 mg	500	522	75	3.23	−2.2
mGL 0.5 mg	501	523	75	3.49	−2.1
mGL 1 mg	502	526	75	3.67	−0.5
DsRed **	559	584	73	3.81	−0.9
DsRed 0.25 mg	559	590	69	3.37	−2.0
DsRed 0.5 mg	559	594	66	5.03	−1.7
DsRed 1 mg	560	613	29	-	−1.3

[a)] Excitation wavelength maximum; [b)] Emission wavelength maximum; [c)] Photoluminescence quantum yield; [d)] Excited state lifetime at 450 nm; [e)] Average excited state lifetime; [f)] Dissymmetry factor.

and **Table 3**). mGL coatings showed a slightly red-shifted emission (7 nm) compared to that in solution, while the excited state lifetime (τ) decay fits better to a mono-exponential equation instead of the common bi-exponential equation in solution. Here, the faster component is identified with the B anionic form and the slower component with the I form of the chromophore.[76–78] The absence of the faster component and the redshifted emission band suggest that the chromophore is in its emissive I form. More importantly, the ϕ is not affected (Table 3). The absorption spectra of the films reveal a very low scattering in the visible range with no appreciable change in the absorption spectrum of mGL (Figure S9 a, Supporting Information). This allows us to determine the CPL properties in the thin-films. In short, g_{lum} values increase up to -2.2×10^{-2} compared to that in solution (Figure 6 and Table 3). This holds up to mGL loadings of 0.5 mg, while the CPL signal is significantly reduced at higher amounts (1 mg) as shown in Figure 6 and Table 3. The increase of the mGL amount does not promote more scattering on the films (Figure S9a, Supporting Information), rather than a more prominent protein-protein interaction (agglomeration) as indicated by the further increased τ and red-shifted emission wavelength maxima.[79] Similar behavior has been already noted for CNC coatings, in which the dilution of the emitter resulted in a higher $g_{lum.}$[80] For reference purposes, we also carried out a control using polyvinylalcohol (PVA) polymer coating that has been used to stabilize CPL emitters in the solid state[81] and recently FPs for lighting devices.[82] Here, the FP-loading threshold to detect CPL signal was as low as 0.01 mg, reaching a g_{lum} of -0.6×10^{-2} (Figure S10, Supporting Information). Further, an increase in mGL loading leads to undetectable CPL, confirming the beneficial effect of HPC and its nematic crystal structure toward developing FP-polymer filters to encode CPL signals in lighting devices. Unfortunately, the remaining FP-polymer down-converting class applied to protein-based hybrid lighting devices is based on a mixture of branched and linear polyethylene oxide that leads to an opaque coating unsuitable for CPL detection.[79,83,84]

Likewise mGL coatings, we noted a slightly red-shifted (6 nm) emission in the DsRed films (Figure 6 and Table 3). However, both the ϕ and τ are slightly reduced compared to those values in solution (Table 3). These changes are typically related to the easy agglomeration of DsRed due to its tetrameric nature, affecting the excitonic interaction between protein subunits. This is also confirmed by i) the decreased thermodynamic stability of DsRed in the HPC matrix, featuring a reduced T_m and T_{nr} with respect to those in solution (Figure S9e,f, Supporting Information), and ii) the further red-shift of the emission maximum wavelength and reduction of the photoluminescence properties upon increasing DsRed loading. At low DsRed loading (0.25 mg), the g_{lum} of the coatings feature a remarkable value of -2×10^{-2}. Unfortunately, further increase of the DsRed loading led to a gradual decrease of these parameters, despite the reduction of ϕ (i.e., -1.7×10^{-2}/66% (0.5 mg) and -1.3×10^{-2}/29% (1 mg)).

The reduction in CPL intensity in both films observed at increasingly higher protein concentrations arises from the increase in protein structural perturbation due to the more protein-protein interaction (protein agglomeration). This is clearly noted in the increase in τ values that are related to changes in its conformation and environment,[79,85] resulting in reduced ϕ and CPL signal. Finally, the protein loading seems to exert a less significant effect in HPC coatings than in PVA films. This could be related to i) better interaction between protein-HPC preserving the native structure or ii) the presence of right-handed chiral nematic phase of HPC that preserves the CPL signal.

2.4. Encoding Protein CPL in Monochromatic and White Lighting Devices

The next question was whether the above FP-coatings were able to keep their polarization capacity over time under constant irradiation stress. Thus, the low-loaded FP coatings (0.25 mg) were deposited onto a blue-emitting LED chip operating to provide a photon flux excitation of 7 mW cm^{-2} (see Experimental Section). At these excitation conditions, the emission band intensity related to the FPs was easily monitored over time, while the CPL signal was measured for each film at certain times (**Figure 7**). Importantly, the g_{lum} holds constant even when 80% loss of the emission intensity is present for both FPs, indicating the CPL signal holds constant over time. CPL is a differential value that arises from emitting proteins and, in turn, reducing the population of emissive proteins through photobleaching does not affect the CPL intensity of the remaining active proteins in the film. This phenomenon is analogous to that observed in photoswitchable proteins, where the photoswitching speed remains constant despite the photobleaching.[86,87]

Next, we tried to realize a broad polarized emission band covering the whole visible range with the combination of both FPs. Attempts to incorporate both proteins in the same film yield a strong Förster resonance energy transfer phenomenon that makes CPL undetectable. To solve this issue, we used a cascade approach, placing a mGL film and a DsRed film on top of each other, where the DsRed film is first excited by the 450 nm light source, leaving enough light to pass through to excite the mGL film. This approach yields a strong CPL signal in the green region and a decreased signal in the DsRed emission region due to the architecture of the cascade coating. With this device structure, we tried to optimize the performance taking advantage of potential enhancement parameters, namely i) an increased

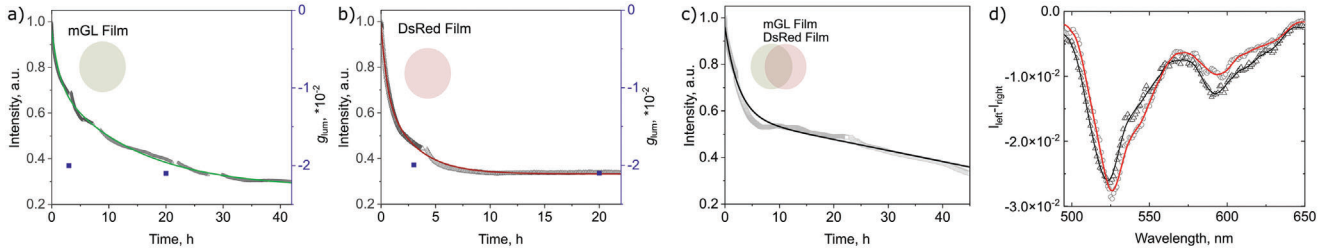

Figure 7. Intensity decay of the FP-HPC materials and g_{lum} spectra of the cascade device over time with their respective film sketches of: a) mGL-HPC 0.25 mg, b) of DsRed-HPC 0.25 mg, c) coupled DsRed and mGL-HPC films each 0.25 mg. d) CPL signal at 0 h (red) and 22 h (black) of coupled DsRed-mGL-HPC films.

content of HPC that can enhance the g_{lum} like reported for CNCs, and ii) separate layers that can enhance the g_{lum} luminophore-independently. Unfortunately, we were unable to fabricate pure color down-converting HLEDs with encoded CPL signal as this feature gets lost upon increasing FP loading (vide supra) that is required to reach a full conversion of the pumping LED. Indeed, though the FP emission can be monitored, the color corruption (Δx and Δy are ≤ 0.02) and luminous efficiency variation (ca. 20%) of monochromatic (450, 520, and 590 nm) and white LEDs are minor in a broad range of operation conditions (10–200 mA), while a stable CPL encoded signal is always successfully integrated (Figures S11 and S12, Supporting Information).

3. Conclusion

This work sets in FPs as a relevant class of CMs with record average B_{CPL} compared to classical small molecules, supramolecular dimers, and d-complexes. In ligand-based FPs, the CPL signal arises from both the protein environment and how the chromophore conformation is locked. In β-barrel FPs, their isolated chromophore already exhibits good g_{lum}, but poor ϕ and ε values. The protein environment leads to a significant increase in these photoluminescence parameters while maintaining the g_{lum}. This results in an average B_{CPL} of $|200|$ $M^{-1}cm^{-1}$ with peak B_{CPL} of -425 and -239 $M^{-1}cm^{-1}$ for the green- (mGL) and red-emitting (DsRed) regions. Thus, this type of CM does not follow the standard correlation between ϕ and g_{lum}. We highlighted the complex interplay between chromophore rigidity, surrounding amino acids, supramolecular packaging, and exciton coupling along several FP examples. Ongoing work is devoted to elucidate the role of each parameter in the CPL signal in solution. Likewise, it is expected that a further enhancement of CPL signal will be achieved with a better understanding about the protein-polymer interaction as well as the possibility to investigate supramolecular assemblies and liquid crystals with FPs. Another asset of FPs as CMs is their easy integration into polymer coatings, keeping an excellent g_{lum} factor even under irradiation stress. This contrasts to other CMs, which typically lose their CPL or ϕ in solid-state due to agglomeration phenomena that leads to self-quenching and high scattering, while CPL stability studies are not reported. Here, we showed that the CPL signal can be kept in a good FP loading range, enabling us to fabricate monochromatic and white lighting devices with encoded green-, red-, and white-CPL signals that are stable over time. Further work in our labs moves on increasing FP loading without losing CPL signal to achieve dual-functional color filters (i.e., fully color down-conversion with defined g_{lum}). All-in-all, FPs are a promising CM family with highly relevant CPL behavior in solution and coatings toward simple biogenic CPL protein-lighting systems.

4. Experimental Section

FP Production and Purification: The FPs were expressed in *Escherichia coli* BL21DE3 containing the plasmid pET21a(+) for EGFP, mGL, sfGFP, mCherry, and UnaG, the plasmid pETDuet for iRFP720 and smURFP, as well as the plasmids pQE30_HcRed, pRSETb_dTomato and pET-29b(+)_DsRed. For cultivation the standard lysogeny broth medium (pH 7.4) was used. For bacteria containing the pET21a(+)/pETDuet/pQE30/pET-29b(+) plasmid the following production protocol was used: several days at 16 °C at 200 rpm. Induction with 10 g L^{-1} glycerol and 0.5 mM/1 mM Isopropyl-β-d-thiogalactopyranosid (IPTG). For the green FPs a final chromophore maturation for 90 min at 30 °C was added, while for DsRed the time was prolonged to 3 h at 30 °C. The bacteria containing pRSETb_dTomato were cultivated at 30 °C and 200 rpm after induction with 1 mM IPTG and 10 g L^{-1} Glycerol for several days. After the cultivation the cells were pelleted by centrifugation (4.000 g, 20 min, 4 °C). Before freezing −20 °C, the bacteria were resuspended in 1xPBS pH 7.4, and pelleted again. The cell opening was performed by sonication using an amplitude of 70% and a 1 s pulse time paired with a 1 s pause for a process time of 8 min. The sonication followed a centrifugation step (38.000 g, 1 h, 4 °C) and an affinity purification via a His-Trap column, followed by desalting in 1xPBS. The proteins were concentrated to 10 mg mL^{-1} and frozen in liquid nitrogen before storage at −80 °C.

Experimental Characterization Techniques: Absorption spectra are recorded with an UVvis-2600i spectrophotometer (Shimadzu) from 250 to 900 nm, with scan speed slow, data interval of 1 nm, and 1 nm slit width using an integrating sphere for solid films. Photophysical studies were carried out at room temperature using a FS5 spectrofluorometer (Edinburgh Instruments) using an SC-10 module for solid samples, an SC-05 for liquid samples and SC-30 integrating sphere to determine the ϕ. A time-correlated single photon-counting (TCPSC) module was used to determine τ and evaluated with Origin 2021b (OriginLab Corporation, Northampton, MA, USA). The average τ was calculated based on the following formula:

$$\langle \tau \rangle = \frac{\sum a_i \tau_i^2}{\sum a_i \tau_i} \quad (3)$$

where a_i are the amplitude fractions and τ_i are the lifetimes.[88]

CPL Measurements: The data was recorded using a Olis CPL Solo (Circulary polarized luminescence) spectrometer and the software OlisGlobalWorks. Raw data were processed by in-house Python script that averaged and processed the data with a Savitzky-Golay filtering of the repeated measurements. The final CPL raw curves were fit by the least-squares method

using the LMFIT and SciPy Python toolboxes to the best double gaussian. The FPs are analysed in 1xPBS buffer pH 7.4, except for mCherry where a 20% ACN and 20% DMSO solution were additionally measured. According to the photophysical characteristics different excitation wavelengths were used. For solid samples the solid holder with an angle of 33° was used for HPC materials while for the PVA materials an angle of 50° was used. The CPL brightness was calculated using Equation (1).[10]

Circular Dichroism (CD) Measurements: The spectra were recorded using a JASCO J-710 CD spectrometer. The proteins are in 1xPBS buffer solution pH 7.4, except for mCherry where a 20% ACN and 20% DMSO solution were additionally measured. For the protein chromophore, the samples were measured in a 1 cm cuvette with an absorbance of 1 at the extinction wavelength. In the case of mCherry for the tryptophan analysis, an absorbance of 0.1 at 280 nm and a 0.1 cm cuvette were selected.

Modulated Scanning Fluorimetry: Modulated scanning fluorimetry (MSF) was performed as previously described in literature.[89] The Thermocycler CFX96 Touch Real_time PCR System (Bio-Rad) was employed to perform MSF measurements. One program composed of heating and cooling cycles ranging from 25 to 99 °C was used to measure the progressive loss of fluorescence and the irreversible unfolding of the FPs studied in this work. The samples were heated 5 °C sec^{-1} and held for 1 min at the temperature peak, followed by a recovery period of 5 min at 25 °C. The thermograms were buffer-subtracted and normalized by the highest fluorescence intensity of each sample. Data analysis was performed using Origin 2021b (OriginLab Corporation, Northampton, MA, USA). Mean values and standard deviations of quintuplicates were calculated and plotted.

Preparation of Protein-Based Materials: HPC (Sigma-Aldrich, M_W ~80 000) was dissolved in Milli-Q water, type I water, with a concentration of 230 mg mL^{-1}. mGL or DsRed-PBS solutions were added to the HPC-solution. After mixing to obtain a homogeneous solution the mixture was drop-casted and dried under ambient conditions via evaporation-induced self-assembly.

Illumination of Protein-Based Materials: The films were placed on top of the LEDs (1 W, WINGER Electronics) with a diffuser (Thorlabs, DG10-220-MD). Electroluminescence spectra, luminous efficiency loss, and color coordinates were recorded with AvaSpec-2048L spectrophotometer and an AvaSphere-30 integrating sphere. To measure the FP intensity decay a shortpass filter with a cut-off wavelength of 450 nm (Thorlabs) was placed between the diffuser and the film to reduce the irradiation intensity to ca. 7 mW cm^{-2}. A 450 nm LED (1 W, WINGER Electronics) was used and driven at 200 mA at ambient conditions in the photostability studies. To operate the LED a Keithley 2231A-30-3 was used.

Computational Characterization Techniques: When crystal structures were unavailable, AlphaFold[90] was used to model molecular structures out of sequence. The chromophore forming residues were replaced by the corresponding chromophore using Coot.[91] Given atomic coordinates for the protein structures of interest, homemade bash and python scripts were used for calculating the average dielectric chromophore according to Li et al. given the amino acid residues within a distance of 5 Å to any of the protein chromophore atoms.[92] For calculating the interplane angles, planes were fitted with homemade bash and python scripts for the imidazolinone and *p*-hydroxybenzyl rings as described in GFPLANE by M. L. Quillin.[93] For both chromophore estimations, the calculations were performed for each member in every population of at least 1000 relaxed protein structures as reported previously.[71,85]

Supporting Information

Supporting Information is available from the Wiley Online Library or from the author.

Acknowledgements

S.G. and M.H. contributed equally to this work. R.D.C., S.G., M.H., S.F., and M.P. acknowledge the European Union's Horizon 2020 research and innovation FET-OPEN under grant agreement ARTIBLED No 863170, the ERC-Co InOutBioLight No. 81685. R.D.C. and J.A.B.V. acknowledge the MSCA-IF grant AnBioLED No 101064305. J.P.F.W. acknowledges the Technical University of Munich under the TUM Seed ERC Funds scheme grant no 2013225. P.B.C. acknowledges financial support under grant PID2021-124080OB-I00 funded by MICIN/AEI/10.13039/501100011033 and ERDF A way of Making Europe. The authors gratefully acknowledge the Gauss Centre for Supercomputing e.V. (www.gauss-centre.eu) for providing computing time on the GCS Supercomputer SuperMuc-NG at Leibniz Supercomputing Centre (www.lrz.de). The authors thank Dr. Julio Fernández Cestau for valuable discussions.

Open access funding enabled and organized by Projekt DEAL.

Conflict of Interest

The authors declare no conflict of interest.

Data Availability Statement

The data that support the findings of this study are available from the corresponding author upon reasonable request.

Keywords

biogenic color filters, circularly polarized luminescence, fluorescent proteins, photon down-conversion, protein-based lighting

Received: January 11, 2024
Revised: March 28, 2024
Published online: May 16, 2024

[1] D. Han, X. Yang, J. Han, J. Zhou, T. Jiao, P. Duan, *Nat. Commun.* **2020**, *11*, 5659.
[2] A. Qu, M. Sun, J.-Y. Kim, L. Xu, C. Hao, W. Ma, X. Wu, X. Liu, H. Kuang, N. A. Kotov, C. Xu, *Nat. Biomed. Eng.* **2020**, *5*, 103.
[3] G. Qian, X. Yang, X. Wang, J. D. Herod, D. W. Bruce, S. Wang, W. Zhu, P. Duan, Y. Wang, *Adv. Opt. Mater.* **2020**, *8*, 2000775.
[4] S.-Y. Yang, Y.-K. Wang, C.-C. Peng, Z.-G. Wu, S. Yuan, Y.-J. Yu, H. Li, T.-T. Wang, H.-C. Li, Y.-X. Zheng, Z.-Q. Jiang, L.-S. Liao, *J. Am. Chem. Soc.* **2020**, *142*, 17756.
[5] Y. Imai, Y. Nakano, T. Kawai, J. Yuasa, *Angew. Chem., Int. Ed.* **2018**, *57*, 8973.
[6] L. E. MacKenzie, R. Pal, *Nat. Rev. Chem.* **2020**, *5*, 109.
[7] J. R. Brandt, F. Salerno, M. J. Fuchter, *Nat. Rev. Chem.* **2017**, *1*, 0045.
[8] E. Gussakovsky, in *Reviews in Fluorescence 2008* (Ed.: C. D. Geddes), Springer, Berlin, Germany **2010**, pp. 425–459.
[9] C. D. Tran, A. F. Drake, *Biochem. Biophys. Rep.* **1981**, *101*, 76.
[10] L. Arrico, L. Di Bari, F. Zinna, *Chem.-Eur. J.* **2021**, *27*, 2920.
[11] Y. Nagata, T. Mori, *Front. Chem.* **2020**, *8*, 448.
[12] C. Tu, W. Wu, W. Liang, D. Zhang, W. Xu, S. Wan, W. Lu, C. Yang, *Angew. Chem., Int. Ed.* **2022**, *61*, e202203541.
[13] Y. Deng, M. Wang, Y. Zhuang, S. Liu, W. Huang, Q. Zhao, *Light Sci. Appl.* **2021**, *10*, 76.
[14] Z.-L. Gong, X. Zhu, Z. Zhou, S.-W. Zhang, D. Yang, B. Zhao, Y.-P. Zhang, J. Deng, Y. Cheng, Y.-X. Zheng, S.-Q. Zang, H. Kuang, P. Duan, M. Yuan, C.-F. Chen, Y. S. Zhao, Y.-W. Zhong, B. Z. Tang, M. Liu, *Sci. China Chem.* **2021**, *64*, 2060.
[15] Y. Wu, M. Li, Z. Zheng, Z.-Q. Yu, W.-H. Zhu, *J. Am. Chem. Soc.* **2023**, *145*, 12951.
[16] J. He, K. Bian, N. Li, G. Piao, *J. Mater. Chem. C* **2019**, *7*, 9278.
[17] X. Wang, B. Zhao, J. Deng, *Adv. Mater.* **2023**, 2304405.

[18] H. Zheng, W. Li, W. Li, X. Wang, Z. Tang, S. X. Zhang, Y. Xu, *Adv. Mater.* **2018**, *30*, 1705948.
[19] European Commission, https://www.photonics21.org/ (accessed: December 2023).
[20] M. Torculas, J. Medina, W. Xue, X. Hu, *ACS Biomater. Sci. Eng.* **2016**, *2*, 1211.
[21] M. Chen, X. Fu, Z. Chen, J. Liu, W. Zhong, *Adv. Funct. Mater.* **2021**, *31*, 2006744.
[22] V. Fernández-Luna, P. B. Coto, R. D. Costa, *Angew. Chem., Int. Ed.* **2018**, *57*, 8826.
[23] J. P. Fuenzalida-Werner, K. Mishra, M. Stankevych, U. Klemm, V. Ntziachristos, A. C. Stiel, *Photoacoustics* **2022**, *25*, 100301.
[24] E. Fresta, V. Fernández-Luna, P. B. Coto, R. D. Costa, *Adv. Funct. Mater* **2018**, *28*, 1707011.
[25] S. Sadeghi, R. Melikov, D. Conkar, E. N. Firat-Karalar, S. Nizamoglu, *Adv. Mater. Technol.* **2020**, *5*, 2000061.
[26] C. P. A. Carlos, S. F. H. Correia, M. Martins, O. A. Savchuk, J. A. P. Coutinho, P. S. André, J. B. Nieder, S. P. M. Ventura, R. A. S. Ferreira, *Green Chem.* **2020**, *22*, 4943.
[27] V. Adam, H. Mizuno, A. Grichine, J. Hotta, Y. Yamagata, B. Moeyaert, G. U. Nienhaus, A. Miyawaki, D. Bourgeois, J. Hofkens, *J. Biotech.* **2010**, *149*, 289.
[28] C. P. Dietrich, A. Steude, L. Tropf, M. Schubert, N. M. Kronenberg, K. Ostermann, S. Höfling, M. C. Gather, *Sci. Adv.* **2016**, *2*, e1600666.
[29] K. Mishra, J. P. Fuenzalida-Werner, F. Pennacchietti, R. Janowski, A. Chmyrov, Y. Huang, C. Zakian, U. Klemm, I. Testa, D. Niessing, V. Ntziachristos, A. C. Stiel, *Nat. Biotechnol.* **2022**, *40*, 598.
[30] J. Dou, A. A. Vorobieva, W. Sheffler, L. A. Doyle, H. Park, M. J. Bick, B. Mao, G. W. Foight, M. Y. Lee, L. A. Gagnon, L. Carter, B. Sankaran, S. Ovchinnikov, E. Marcos, P.-S. Huang, J. C. Vaughan, B. L. Stoddard, D. Baker, *Nature* **2018**, *561*, 485.
[31] A. Kumagai, R. Ando, H. Miyatake, P. Greimel, T. Kobayashi, Y. Hirabayashi, T. Shimogori, A. Miyawaki, *Cell* **2013**, *153*, 1602.
[32] J. P. Fuenzalida-Werner, R. Janowski, K. Mishra, I. Weidenfeld, D. Niessing, V. Ntziachristos, A. C. Stiel, *J. Struct. Biol.* **2018**, *204*, 519.
[33] J. A. J. Arpino, P. J. Rizkallah, D. D. Jones, *PLoS One* **2012**, *7*, e47132.
[34] J. L. Tubbs, J. A. Tainer, E. D. Getzoff, *Biochem* **2005**, *44*, 9833.
[35] E. A. Rodriguez, G. N. Tran, L. A. Gross, J. L. Crisp, X. Shu, J. Y. Lin, R. Y. Tsien, *Nat. Methods* **2016**, *13*, 763.
[36] D. M. Shcherbakova, V. V. Verkhusha, *Nat. Methods* **2013**, *10*, 751.
[37] X. Cao, C. Zhang, Z. Gao, Y. Liu, Y. Zhao, Y. Yang, J. Chen, R. Jimenez, J. Xu, *Phys. Chem. Chem. Phys.* **2019**, *21*, 2365.
[38] G. Blauer, G. Wagniere, *J. Am. Chem. Soc.* **1975**, *97*, 1949.
[39] R. V. Person, B. R. Peterson, D. A. Lightner, *J. Am. Chem. Soc.* **1994**, *116*, 42.
[40] C. Tran, G. S. Beddard, *J. Am. Chem. Soc.* **1982**, *104*, 6741.
[41] F. S. Richardson, J. P. Riehl, *Chem. Rev.* **1977**, *77*, 773.
[42] J. F. Towell, R. W. Woody, *Biochem* **1980**, *19*, 4231.
[43] Q. Jiang, X. Xu, P.-A. Yin, K. Ma, Y. Zhen, P. Duan, Q. Peng, W.-Q. Chen, B. Ding, *J. Am. Chem. Soc.* **2019**, *141*, 9490.
[44] P. A. Zunszain, J. Ghuman, A. F. McDonagh, S. Curry, *J. Mol. Biol.* **2008**, *381*, 394.
[45] A. Remeeva, K. Kovalev, I. Gushchin, A. Fonin, K. Turoverov, O. Stepanenko, RCSB PDB **2023**, https://doi.org/10.2210/pdb8AFK/pdb.
[46] N. V. Visser, M. A. Hink, J. W. Borst, G. N. M. Van Der Krogt, A. J. W. G. Visser, *FEBS Lett.* **2002**, *521*, 31.
[47] K. J. Fujimoto, K. Inoue, *J. Chem. Phys.* **2020**, *153*, 045101.
[48] G. Pescitelli, *Chirality* **2022**, *34*, 333.
[49] S. Matile, N. Berova, K. Nakanishi, J. Fleischhauer, R. W. Woody, *J. Am. Chem. Soc.* **1996**, *118*, 5198.
[50] E. Krissinel, K. Henrick, *J. Mol. Biol.* **2007**, *372*, 774.
[51] J.-D. Pédelacq, S. Cabantous, T. Tran, T. C. Terwilliger, G. S. Waldo, *Nat. Biotechnol.* **2006**, *24*, 79.
[52] B. C. Campbell, E. M. Nabel, M. H. Murdock, C. Lao-Peregrin, P. Tsoulfas, M. G. Blackmore, F. S. Lee, C. Liston, H. Morishita, G. A. Petsko, *Proc. Natl. Acad. Sci. U. S. A.* **2020**, *117*, 30710.
[53] A. Pikulska, A. H. Steindal, M. T. P. Beerepoot, M. Pecul, *J. Phys. Chem. B* **2015**, *119*, 3377.
[54] C. A. Ullrich, *Time-Dependent Density-Functional Theory: Concepts and Applications*, Oxford University Press, Oxford, UK **2011**.
[55] J. Tong, Y. Cao, Y. Zhang, P. Wang, P. Wang, X. Liao, W. Zhang, Y. Wang, Y. Zheng, J. Zhu, Y. Pan, *Angew. Chem., Int. Ed.* **2022**, *61*, e202209438.
[56] N. C. Shaner, R. E. Campbell, P. A. Steinbach, B. N. G. Giepmans, A. E. Palmer, R. Y. Tsien, *Nat. Biotechnol.* **2004**, *22*, 1567.
[57] M. V. Matz, A. F. Fradkov, Y. A. Labas, A. P. Savitsky, A. G. Zaraisky, M. L. Markelov, S. A. Lukyanov, *Nat. Biotechnol.* **1999**, *17*, 969.
[58] N. G. Gurskaya, A. F. Fradkov, A. Terskikh, M. V. Matz, Y. A. Labas, V. I. Martynov, Y. G. Yanushevich, K. A. Lukyanov, S. A. Lukyanov, *FEBS Lett.* **2001**, *507*, 16.
[59] G. Sánchez-Mosteiro, M. Koopman, E. M. H. P. Van Dijk, J. Hernando, N. F. Van Hulst, M. F. García-Parajó, *ChemPhysChem* **2004**, *5*, 1782.
[60] J. P. Fuenzalida Werner, Y. Huang, K. Mishra, R. Janowski, P. Vetschera, C. Heichler, A. Chmyrov, C. Neufert, D. Niessing, V. Ntziachristos, A. C. Stiel, *Anal. Chem.* **2020**, *92*, 10717.
[61] M. F. Garcia-Parajo, M. Koopman, E. M. H. P. van Dijk, V. Subramaniam, N. F. van Hulst, *Proc. Natl. Acad. Sci. U. S. A.* **2001**, *98*, 14392.
[62] P. G. Wilmann, J. Petersen, A. Pettikiriarachchi, A. M. Buckle, S. C. Smith, S. Olsen, M. A. Perugini, R. J. Devenish, M. Prescott, J. Rossjohn, *J. Mol. Biol.* **2005**, *349*, 223.
[63] X. Shu, N. C. Shaner, C. A. Yarbrough, R. Y. Tsien, S. J. Remington, *Biochem* **2006**, *45*, 9639.
[64] P. P. Chapagain, C. K. Regmi, W. Castillo, *J. Chem. Phys.* **2011**, *135*, 235101.
[65] A. Acharya, A. M. Bogdanov, B. L. Grigorenko, K. B. Bravaya, A. V. Nemukhin, K. A. Lukyanov, A. I. Krylov, *Chem. Rev.* **2017**, *117*, 758.
[66] M. Andresen, A. C. Stiel, S. Trowitzsch, G. Weber, C. Eggeling, M. C. Wahl, S. W. Hell, S. Jakobs, *Proc. Natl. Acad. Sci. U. S. A.* **2007**, *104*, 13005.
[67] M. G. Khrenova, F. D. Mulashkin, A. V. Nemukhin, *J. Chem. Inf. Model.* **2021**, *61*, 5125.
[68] J. D. Fradgley, A. T. Frawley, R. Pal, D. Parker, *Phys. Chem. Chem. Phys.* **2021**, *23*, 11479.
[69] M. Ikeshita, H. He, M. Kitahara, Y. Imai, T. Tsuno, *RSC Adv.* **2022**, *12*, 34790.
[70] D. Shcherbo, E. M. Merzlyak, T. V. Chepurnykh, A. F. Fradkov, G. V. Ermakova, E. A. Solovieva, K. A. Lukyanov, E. A. Bogdanova, A. G. Zaraisky, S. Lukyanov, D. M. Chudakov, *Nat. Methods* **2007**, *4*, 741.
[71] M. Hasler, M. Patrian, J. A. Banda-Vázquez, S. Ferrara, A. C. Stiel, J. Fuenzalida-Werner, R. D. Costa, *Adv. Funct. Mater.* **2023**, 2301820.
[72] C. L. C. Chan, M. M. Bay, G. Jacucci, R. Vadrucci, C. A. Williams, G. T. Van De Kerkhof, R. M. Parker, K. Vynck, B. Frka-Petesic, S. Vignolini, *Adv. Mater.* **2019**, *31*, 1905151.
[73] C. Duan, Z. Cheng, B. Wang, J. Zeng, J. Xu, J. Li, W. Gao, K. Chen, *Small* **2021**, *17*, 2007306.
[74] G. Charlet, D. Gray, *J. Appl. Polym. Sci.* **1989**, *37*, 2517.
[75] H. Zheng, B. Ju, X. Wang, W. Wang, M. Li, Z. Tang, S. X. Zhang, Y. Xu, *Adv. Opt. Mater.* **2018**, *6*, 1801246.
[76] G. Striker, V. Subramaniam, C. A. M. Seidel, A. Volkmer, *J. Phys. Chem. B* **1999**, *103*, 8612.
[77] S. Völker, T. M. H. Creemers, A. J. Lock, V. Subramaniam, T. M. Jovin, *Nat. Struct. Biol.* **1999**, *6*, 557.
[78] M. Cotlet, J. Hofkens, M. Maus, T. Gensch, M. Van Der Auweraer, J. Michiels, G. Dirix, M. Van Guyse, J. Vanderleyden, A. J. W. G. Visser, F. C. De Schryver, *J. Phys. Chem. B* **2001**, *105*, 4999.

[79] V. Fernández-Luna, D. Sánchez-de Alcázar, J. P. Fernández-Blázquez, A. L. Cortajarena, P. B. Coto, R. D. Costa, *Adv. Funct. Mater.* **2019**, *29*, 1904356.
[80] G. Wei, M. Lu, K. Feng, S. Ma, Y. Jiang, Z. Jin, *ACS Omega* **2023**, *8*, 23191.
[81] H. Zhong, B. Zhao, J. Deng, *Adv. Opt. Mater.* **2023**, *11*, 2202787.
[82] S. Ferrara, J. P. Fernandéz-Blázquez, J. P. Fuenzalida Werner, R. D. Costa, *Adv. Funct. Mater.* **2023**, *33*, 2300350.
[83] M. D. Weber, L. Niklaus, M. Pröschel, P. B. Coto, U. Sonnewald, R. D. Costa, *Adv. Mater.* **2015**, *27*, 5493.
[84] S. Ferrara, S. H. Mejias, M. Liutkus, G. Renno, F. Stella, I. Kociolek, J. P. Fuenzalida-Werner, C. Barolo, P. B. Coto, A. L. Cortajarena, R. D. Costa, *Adv. Funct. Mater.* **2022**, *32*, 2111381.
[85] M. Patrian, M. Nieddu, J. A. Banda-Vázquez, D. Gutierrez-Armayor, G. González-Gaitano, J. P. Fuenzalida-Werner, R. D. Costa, *Adv. Mater.* **2023**, *35*, 2303993.
[86] P. Vetschera, K. Mishra, J. P. Fuenzalida-Werner, A. Chmyrov, V. Ntziachristos, A. C. Stiel, *Anal. Chem.* **2018**, *90*, 10527.
[87] M. Andresen, A. C. Stiel, J. Fölling, D. Wenzel, A. Schönle, A. Egner, C. Eggeling, S. W. Hell, S. Jakobs, *Nat. Biotechnol.* **2008**, *26*, 1035.
[88] A. Sillen, Y. Engelborghs, *Photochem. Photobiol.* **1998**, *67*, 475.
[89] H. L. Svilenov, T. Menzen, K. Richter, G. Winter, *Mol. Pharmaceutics* **2020**, *17*, 2638.
[90] J. Jumper, R. Evans, A. Pritzel, T. Green, M. Figurnov, O. Ronneberger, K. Tunyasuvunakool, R. Bates, A. Žídek, A. Potapenko, A. Bridgland, C. Meyer, S. A. A. Kohl, A. J. Ballard, A. Cowie, B. Romera-Paredes, S. Nikolov, R. Jain, J. Adler, T. Back, S. Petersen, D. Reiman, E. Clancy, M. Zielinski, M. Steinegger, M. Pacholska, T. Berghammer, S. Bodenstein, D. Silver, O. Vinyals, et al., *Nature* **2021**, *596*, 583.
[91] P. Emsley, B. Lohkamp, W. G. Scott, K. Cowtan, *Acta Crystallogr. D Biol. Crystallogr.* **2010**, *66*, 486.
[92] L. Li, C. Li, Z. Zhang, E. Alexov, *J. Chem. Theory Comput.* **2013**, *9*, 2126.
[93] M. L. Quillin, D. M. Anstrom, X. Shu, S. O'Leary, K. Kallio, D. M. Chudakov, S. J. Remington, *Biochem* **2005**, *44*, 5774.